

Detection of large-scale cosmological dark matter structure via gravitational lens distortion

David M. Wittman, J. Anthony Tyson, David Kirkman,
Ian Dell'Antonio^y, and Gary Bernstein^z

February 23, 2019

Bell Laboratories, Lucent Technologies, Murray Hill, NJ 07574

^y Kitt Peak National Observatory, NOAO, Tucson, Arizona 85726

^z Astronomy Department, University of Michigan, Ann Arbor, MI 48109

Most of the matter in the universe is not luminous and can be observed directly only through its gravitational effect. The large-scale distribution of this dark matter is a fundamental issue in cosmology, because it tells us about global cosmological parameters and about the nature of the dark matter. A new technique called weak gravitational lensing uses background galaxies to reveal the foreground dark matter distribution on large scales. Light from very distant galaxies travels to us through many intervening overdensities which gravitationally distort their apparent shapes. The observed ellipticity pattern of distant galaxies thus encodes information about the large-scale structure of the universe, but attempts to measure this effect have been inconclusive due to systematic errors. We report the first detection of this "cosmic shear" using 145,000 background galaxies to reveal the dark matter distribution on angular scales up to half a degree in three separate lines of sight. The observed angular dependence of this effect is consistent with that predicted by two leading cosmological models, providing new and independent support for these models.

To date, most of what we know about the large-scale structure of the universe comes from the observed anisotropies in the cosmic microwave background (CMB) and from the distribution of galaxies. The CMB provides the earliest sample of mass fluctuations, from a time when the universe was a 100,000 times younger.¹ Different cosmological models predict different scenarios in the growth of mass structures over cosmic time, so comparing the CMB-derived mass spectrum with that seen at later times will be a powerful test of cosmology. The large-scale mass distribution at late times has traditionally been characterized through the large-scale galaxy distribution on the assumption that light traces mass.

The distribution of this dark mass can be investigated more directly via its gravitational effects on the appearance of background galaxies. Any foreground mass bends light rays from a distant source, moving the apparent position of the source to a new position on the sky and stretching its image tangentially, by an amount proportional to the foreground mass. This weak lensing effect has already been used to study the mass distribution within clusters of galaxies, where the large mass associated with the clusters makes the gravitationally induced ellipticity of the background galaxies easily detectable.^{2,17} In principle, weak lensing can also tell us about large-scale structure through the cumulative effect of many intervening overdensities. A deep image of a patch of the sky looks out through the three-dimensional forest of galaxies seen in projection: any two galaxies are most likely not physical neighbors and, absent lensing, their projected shapes or ellipticities are statistically uncorrelated. In the presence of foreground mass overdensities, the light rays from galaxies narrowly separated on the sky travel similar paths past intervening mass concentrations and thus undergo similar image distortions. The resulting correlation of distant galaxy ellipticities is highest at small angular separation and drops for widely separated galaxies whose light bundles travel through completely different structures (Fig. 1).

Theoretical expectations for this "cosmic shear" on the 10–30 arcminute angular scales of large-scale mass structure range from a few percent for standard cold dark matter to less than one percent for an open universe which would expand forever.^{8,9,10,11,12,13,14} The typical background galaxy has an ellipticity of roughly 30% so that many thousands of source galaxies must be averaged together to detect the small cosmic shear. Earlier attempts to measure it were inconclusive,^{16,17,18} with the main difficulty

being control of systematic errors in galaxy shapes arising from the optical system or the process of observation. The earliest attempts with photographic plates, while covering a large field, suffered from plate-to-plate systematicatics as well as nonlinearity and lack of sensitivity. With the advent of much more sensitive and linear charge-coupled devices (CCDs), the small field size covered by these devices became a problem.

We have imaged large areas of sky in several directions using a mosaic of CCDs on a large telescope, covering hundreds of thousands of distant galaxies at multiple wavelengths. We describe the steps taken to minimize systematic errors and to select 145,000 of the most reliable distant galaxy measurements. We find significant ellipticity correlations on angular scales of 0.03°–0.5°. This is the first direct probe of the aggregate mass distribution in the universe on the several billion light-year scale, and the results are consistent with two leading cosmological models.

Wide-field imaging with control of systematic shape errors

We observed three "blank" (i.e., not containing any known mass concentrations) fields at $23^h 48^m$, $+00^{\circ} 57^0$ J2000; $04^h 29^m$, $-36^{\circ} 18^0$; and $11^h 38^m$, $-12^{\circ} 33^0$ over a period of several years, using the Big Throughput Camera,²⁰ an array of four large charge-coupled devices (CCDs) at the Cerro Tololo Inter-American Observatory's 4-m Blanco telescope. This camera covers a 35 arcmin square field of view with 0.43 arcsecond pixels, and we took multiple 500 second exposures shifted by 5-7 arcmin inutes and combined them to cover a 43 arcmin square field. Before combining, we took several steps to reduce systematic errors arising from anisotropy in the response of the optical system to point sources. First, we registered all the images onto a common linear coordinate system, free of the known radial distortion of the telescope optics. We then used the shapes of stars, which are foreground point sources free of the gravitational lensing effect, to correct any additional point-spread function anisotropies such as those due to astigmatism and guiding errors.

The shape of a star or galaxy can be described by its second central moments, $I_{xx} = \sum w x^2$, $I_{yy} = \sum w y^2$, and $I_{xy} = \sum w xy$, where $I(x; y)$ is the intensity distribution above the night sky level, $w(x; y)$ is a weight function, the sum is over a contiguous set of pixels defined as belonging to the galaxy, and the coordinate system has been translated so that the first moments vanish. The second moments can be combined to form a size, $I_{xx} + I_{yy}$, and two components of a pseudo-vector ellipticity, $e_1 = (I_{xx} - I_{yy}) / (I_{xx} + I_{yy})$ and $e_2 = 2I_{xy} / (I_{xx} + I_{yy})$, which vary in the range [-1; 1] (ellipticity in its colloquial sense is the amplitude of this pseudo-vector, $\sqrt{e_1^2 + e_2^2}$ with its range [0; 1]). Traditional intensity-weighted moments are calculated with $w = 1$, but this produces ellipticity measurements with noise properties that are far from optimal or even divergent. We use an elliptical Gaussian as the weight function, which places more weight on the high-signal-to-noise inner parts of the galaxy image, and is nearly optimal for most point-spread functions and for typical exponential galaxy profiles.

The moments of the Gaussian weight ellipse are iterated (from initial values provided by unweighted moments) to match the size and shape of

the object, in order to obtain the highest possible signal-to-noise and to insure that the measured ellipticity is not biased toward the shape of the weight function. The iteration may fail to converge for very noisy galaxy images or for galaxies with near neighbors, but such objects generally carry little information on lensing. This "adaptively weighted moments" scheme has been extensively tested on simulated and real data, and has been shown to be unbiased, and substantially more accurate than unweighted or circularly-weighted methods.²¹ For objects which survive the convergence test, the measurement error in the malellipticity is accurately estimated by propagating the Poisson photon noise through the moment equations. The remaining objects are excluded from the analysis.

Stars are distinguished from galaxies by their clear separation at the bright end of a size-density diagram. We identified roughly 100 such stars on each exposure of each CCD and did a least-squares fit (with 3-clip) of a second-order polynomial to the spatial variation of their ellipticity components $e_1(x;y)$ and $e_2(x;y)$, which would be zero at all points in an ideal observation free of point-spread function anisotropy. Fischer and Tyson²² have shown that nonzero e_1 and e_2 can be cancelled by convolution with a small (three pixel square) flux-conserving kernel with ellipticity components equal and opposite to those of the stars. We convolved each image with its resulting position-dependent kernel, after which the stellar ellipticities show little variation as a function of position, and $h_{e_1}i$ and $h_{e_2}i$ (where brackets indicate averaging over all the stars in an image) typically fall from a few percent to a few tenths of a percent. We then combined the images by averaging with a 3-clip, and repeated the point-spread function rounding on the combined image (using roughly 1000 stars and a fourth-order polynomial in this case). This last step typically reduced $h_{e_1}i$ and $h_{e_2}i$ over the 43 arcminute image to a few hundredths of a percent; more specific checks for systematic error will be derived below.

Catalogues of distant galaxies

We repeated the observing and image processing for each field in three wavelength bands centered on 450 nm, 650 nm, and 850 nm, and for two of the fields we also took 550 nm images. The mean exposure time at each wavelength was 3400 sec. In each field, we used standard software²³ to

identify object positions and fluxes on the 650 nm image, yielding roughly 150,000 objects per field. At each object's position, we evaluated the weighted moments at each wavelength, retaining only the measurements which the iterative weighted moment algorithm did not flag as suspect (by far the most common flag is for centroid shift from the starting position, indicating possible contamination from neighboring objects.) Measurements with small sizes ($I_{xx} < 1.0$ or $I_{yy} < 1.0$) were also excluded as suspect. The result is a list of multiple independent ellipticity measurements (and corresponding estimated measurement errors ϵ_i) for each object.

We then computed the best estimate of each galaxy's ellipticity by averaging the remaining measurements, weighted inversely by their estimated errors. If either of the ellipticity components at any wavelength deviated from this mean by more than $3\epsilon_i$, that wavelength was eliminated and the process repeated. This step thus eliminates individual galaxy ellipticity measurements at wavelengths at which objects were noisy or blended, and it also reduces the systematic errors because the images at different wavelengths do not share the same residual point-spread function anisotropy. Finally we rejected objects with $\epsilon_i > 0.6$ as likely to be blends of more than one object, and applied flux density criteria (1.8 Jy $> F_i > 0.11$ Jy through the 650 nm filter, 23.26 magnitude) to select objects likely to be distant galaxies. We use these same selection criteria in calibrating the mean redshift of the background galaxies (below). The final catalogues contain about 45,000 galaxies in each field.

These observed ellipticities must be corrected for the overall broadening effect of the point-spread function, which makes elliptical galaxies appear more circular even if the point-spread function itself is perfectly isotropic. To calibrate this effect, we took a deep image with a very small point spread (the Hubble Deep Field South) and convolved it to the resolution of our final images, which is 1.07{1.25 arcsec as measured by the full width at half-maximum at 650 nm. (The resolution on individual exposures, or "seeing" was better, but the stellar size is larger in the final image with systematic shape errors removed from the point-spread function.) While some isolated galaxies became broader and less elliptical as predicted, many merged with their neighbors, making it impossible an accurate extrapolation from observed to true ellipticity. Instead of attempting this extrapolation for individual galaxies, we distorted the Hubble Deep Field

South with a known shear, convolved and added noise to match our images, and measured the mean ellipticity of galaxies in our flux density range. The ratio of induced to recovered ellipticity was 45/05.

Ellipticity correlations of distant galaxies

Miralda-Escude¹⁰ has defined two physically revealing ellipticity correlation functions. In this approach, the ellipticity components of a galaxy i are calculated not with respect to the arbitrary x and y axes of the image, but with respect to the line joining it to another galaxy j (Fig. 2). Averaging over all galaxies i and j separated by angle θ on the sky, the correlations $\langle \epsilon_1 \epsilon_{1,j} \rangle_i$ and $\langle \epsilon_2 \epsilon_{2,j} \rangle_i$ have a unique signature in the presence of gravitational lensing, explained in detail in Fig. 2.

Figure 3 shows the ellipticity correlations in the angular separation range 2–36 arcmin, averaged over the three fields (red). The errors plotted are 1 errors in the mean derived from the variance among the fields. Some “cosmic variance”, or real systematic differences among fields of this size, is expected, so that these errors include both measurement error and cosmic variance. The measurement errors on ϵ_1 and ϵ_2 are statistically independent. The signature of gravitational lensing by large-scale structure is evident: ϵ_1 declines as the angular scale increases, but is positive at all scales, while ϵ_2 matches ϵ_1 at small scales but drops below zero at large scales.

We performed several tests to rule out systematic errors. The effects of residual point-spread function anisotropy are demonstrated by plotting the correlation functions of the stars (blue), which are far closer to zero than are the galaxy correlations. To check that stars not used in the point-spread function calibration also have zero correlations, we selected a disjoint sample of objects likely to be late M-dwarf stars based on their colours. These objects are several times fainter on average than the calibration stars, and some are as faint as the background galaxies. A restrictive colour selection presumably with few interloping galaxies yields roughly 300 stars in each of the two fields for which we have data at four wavelengths. Their correlation functions are consistent with those of the point-spread function calibration stars. A test involving the background galaxy sample is to rotate each galaxy by 45° and ensure that the effect vanishes. This is equivalent to the cross correlation $\frac{1}{2}(\epsilon_{1,j} \epsilon_{2,j} + \epsilon_{2,j} \epsilon_{1,j})$, which is also plotted in Figure 3 (black). The result is reassuringly close to zero. The scatter in the cross correlation can also be taken as an indicator of the statistical error associated with the number and distribution of

galaxies included in the catalogues.

Apart from these null tests, there are also alternative tests. First, the mass of the aperture mass,²⁴ an indicator of the inhomogeneity of the foreground mass, computed from the same catalogues falls within expectations (from 12% for 4 arcmin diameter apertures to 0.5% for 20 arcmin). Second, a 650-nm image of a massive cluster, taken with the same camera and processed in the same way, exhibits correlation functions of the expected angular dependence and of larger amplitude than in any of the three blank fields, despite likely contamination of the galaxy sample by cluster members. All these tests indicate that we have indeed measured cosmic shear. We now turn to comparisons with theoretical predictions of this effect.

Comparison with theoretical predictions

Ellipticity correlations increase strongly with background galaxy redshift, so we must first constrain the source redshift distribution $N(z)$. Very little is known about the redshift distribution of galaxies as faint as those used here, so we assume a simple model $N(z) = z^2 \exp(-z-z_0)$, and adjust z_0 to match lens observations of a high-redshift galaxy cluster of known velocity dispersion (M S1054 at $z = 0.83$).²⁵ We observed this cluster with the BPC and reduced the data in the same way as for the blank fields, and compared the faint galaxy ellipticities (tangential to the cluster center) to that expected for a range of z_0 . We found that $z_0 = 0.5$ was the best match.

This model $N(z)$ was used as input to a cold dark matter simulation code by W. Hu and J. M. Miralda-Escude (see ref²⁶), which computes the shear power spectrum and correlation function for any given cosmology, using the prescription of Hamilton et al.²⁷ and Peacock & Dodds²⁸ to calculate the mass power spectrum in the non-linear regime when the growth of gravitationally collapsed dark matter structures modified the mass spectrum. Results were obtained for three cosmological models and are plotted along with our seeing-corrected measurements on a logarithmic scale in Figure 4. Two current models were normalized to the microwave background fluctuations (COBE) at large angle and to local galaxy cluster abundance (assuming mass traces light) at small angle: an open universe with $\Omega_{\text{matter}} = 0.4$ (red in Figure 4), and a flat universe dominated by a cosmological constant $\Lambda = 0.67$ (green, solid line). The agreement between the data and the two viable cosmological models is impressive for a first measurement. For comparison purposes we also show the old standard cold dark matter cosmology (blue), which is only COBE normalized. (A full listing of the parameters used in these models is shown in Table 1.) To illustrate the effect of varying $N(z)$, we also plot the Λ -dominated cosmology with $z_0 = 0.3$ (green, dotted line). Decreasing z_0 decreases the amplitude of the correlations, but has little effect on their shapes. The uncertainty in $N(z)$ implies a factor of several uncertainty in the interpretation of our measurement, and is by far the dominant calibration error.

Despite this uncertainty, COBE-normalized standard cold dark matter is ruled out by the measured values of τ_1 . While this is not surprising, it is

the first cosmological constraint from wide-field weak lensing, and it agrees with several other methods which disfavor this model^{29,30}. The other two models are consistent with the data at the 2 level. The indication of a low matter universe here is in agreement with a remarkable array of independent methods, including type Ia supernovae, cosmic microwave background anisotropies, cluster baryon fraction together with cluster mass (lensing) and primordial deuterium, and the age of the oldest stars coupled with the Hubble constant.³¹

This technique can further distinguish between open and closed universes if extended to the somewhat larger angular scales where those cosmologies predict Ω_2 will cross zero as shown in Figure 4. A survey of Ω_2 fields now underway will rule out one or more of these cosmologies at the 8 level at 10 arcmin angles (3 level for a differential measure of the slope of the power spectrum). Separating the background galaxies into discrete redshift bins based on multi-colour photometry will enable measurement of the ellipticity correlation (or equivalently the dark matter power spectrum) as a function of cosmological time; wide-field weak lensing surveys deep enough to identify galaxies at $z=2$ and measure their shapes will constrain several cosmological parameters.²⁶ The combination of all the power spectrum probes (lensing, cosmic microwave background, galaxy distributions, and peculiar velocities) will tightly constrain theories of the origins of fluctuations in the early universe and their growth into galaxies and large-scale structure.

Acknowledgments

We gratefully acknowledge help from W. Hu and J.M. Miralda-Escude on theoretical predictions of several cosmological models. We thank Steven Gentile for his artwork. Cerro Tololo Inter-American Observatory is a division of National Optical Astronomy Observatory (NOAO), which is operated by the Association of Universities for Research in Astronomy, Inc., under Cooperative Agreement with the National Science Foundation.

References

¹L. Page and D. T. Wilkinson. The cosmic microwave background. *Rev. Mod. Phys.*, 71:173{179, 1999.

²J. A. Tyson, F. Valdes, and R. Weyn. Detection of systematic gravitational lens galaxy images: mapping dark matter in galaxy clusters. *Astrophys. J.*, 349:L1{L4, 1990.

³G. Fahlman, N. Kaiser, G. Squires, and D. Woods. Dark matter in MS1224 from distortion of background galaxies. *Astrophys. J.*, 437:56{62, 1994.

⁴G. Squires, N. Kaiser, G. Fahlman, A. Babul, and D. Woods. A weak gravitational lensing analysis of Abell 2390. *Astrophys. J.*, 469:73{77, 1996.

⁵D. C. Lowe, G. A. Luppino, N. Kaiser, J. P. Henry, and I. M. Gioia. Weak lensing by two $z = 0.8$ clusters of galaxies. *Astrophys. J.*, 497:61{64, 1998.

⁶H. Hoekstra, M. Franx, K. Kuijken, and G. Squires. Weak lensing analysis of Cl1358+62 using Hubble Space Telescope observations. *Astrophys. J.*, 504:636{660, 1998.

⁷Y. M. Mellier. Probing the universe with weak lensing. *Annu. Rev. Astron. Astrophys.*, 37:127{189, 1999.

⁸J. E. Gunn. A fundamental limitation on the accuracy of angular measurement in observational cosmology. *Astrophys. J.*, 147:61{72, 1967.

⁹C. Dyer and R. Roeder. Observations in locally inhomogeneous cosmological models. *Astrophys. J.*, 189:167{175, 1974.

¹⁰J. M. Maraldie-Escudé. The correlation function of galaxy ellipticities produced by gravitational lensing. *Astrophys. J.*, 380:1{8, 1991.

¹¹R. Blandford, A. Saur, T. Brainerd, and J. V. Gunn. The distortion of distant galaxy images by large scale structure. *Mon. Not. Royal Astron. Soc.*, 251:600{627, 1991.

¹²N. Kaiser. Weak gravitational lensing of distant galaxies. *Astrophys. J.*, 388:272{286, 1992.

¹³J. V. Gunn. Weak lensing by large-scale structure in open, flat and closed universes. *Mon. Not. Royal Astron. Soc.*, 281:369{383, 1996.

¹⁴B . Jain and U . Seljak. Cosmological model predictions for weak lensing. *Astrophys. J.*, 484:560{573, 1997.

¹⁵N . Kaiser. Weak lensing and cosmology. *Astrophys. J.*, 498:26{42, 1998.

¹⁶J. K ristian. On the cosmological distortion effect. *Astrophys. J.*, 147:864{867, 1967.

¹⁷F . Valdes, J.A . Tyson, and J.F . Jarvis. A lignment of faint galaxy images: cosmological distortion and rotation. *Astrophys. J.*, 271:431{441, 1983.

¹⁸J. M ould, R . B landford, J. V illum sen, T . Brainerd, I. Sm ail, T . Sm all, and W . K ells. A search for weak distortions of distant galaxy images by large-scale structure. *Mon. Not. Royal Astron. Soc.*, 271:31{38, 1994.

¹⁹P . Schneider, L . van W aerbeke, Y . M ellier, B . Jain, S . Seitz, and B . Fort. Detection of shear due to weak lensing by large-scale structure. *Astron. Astrophys.*, 333:767{778, 1998.

²⁰D . W ittm an, J.A . Tyson, G .M . Bernstein, R .W . Lee, I.P . Dell'Antonio, P .F ischer, D .R . Sm ith, and M .M . Blouke. Big throughput camera: the first year. *Proc. Soc. Photo-Optical Instr. Eng.*, 3355:626{634, 1998.

²¹et.al. Bernstein, G .M . Optimal methods for weak gravitational lensing. *Astrophys. J.*, 000:in preparation, 2000.

²²P .F ischer and J.A . Tyson. The mass distribution of the most luminous x-ray cluster rxj1347.5-1145 from gravitational lensing. *Astron. J.*, 114:14{24, 1997.

²³E .B ertin and S .A rmouts. SExtractor: software for source extraction. *Astron. Astrophys. Suppl.*, 117:393{404, 1996.

²⁴P . Schneider, L . van W aerbeke, Y . M ellier, B . Jain, S . Seitz, and B . Fort. A new measure for cosm ic shear. *Mon. Not. Royal Astron. Soc.*, 296:873{892, 1998.

²⁵K .H .Tran, D .D .K elson, P .van Dokkum , M .Franx, G .D . Illingworth, and D .M agee. The velocity dispersion of m s1054-03: a massive galaxy cluster at high redshift. *Astrophys. J.*, 522:39{45, 1999.

²⁶W . Hu. Power spectrum tomography with weak lensing. *Astrophys. J.*, 522:L21{L24, 1999.

²⁷A . J . S . H am ilton, A . M atthews, P . K um ar, and E . Lu . Reconstructing the prim ordial spectrum of uctuations of the universe from the observed nonlinear clustering of galaxies. *A strophys. J.*, 374:L1{L4, 1991.

²⁸J . A . Peacock and S . J . D odds. Non-linear evolution of cosm ological power spectra. *M on . Not. Royal A stron . Soc.*, 280:L19{L26, 1996.

²⁹J . P . O stricker and P . J . Steinhardt. The observational case for a low density universe with a cosm ological constant. *N ature*, 377:600{602, 1995.

³⁰N . A . Bahcall, J . P . O stricker, S . Perlmutter, and P . J . Steinhardt. The cosm ic triangle: revealing the state of the universe. *Science*, 284:1481{1488, 1999.

³¹M . S . Turner and J . A . Tyson . Cosm ology at the millennium . *Rev. Mod. Phys.*, 71:145{164, 1999.

³²C . F renk, S . D . M . W hite, G . E ffstathiou, and M . D avis. Galaxy clusters and the amplitude of prim ordial uctuations. *A strophys. J.*, 351:10{21, 1990.

Table 1 Summary of cosmological models

Model	b_b	m_{matter}	b_b	H_0	n	σ_8	normalization
Standard cold dark matter	.05	.95	0	50	1.0	1.17	COBE only
-dominated, at	.039	.291	.67	70	0.94	0.84	COBE + clusters
Open universe	0.045	0.405	0	65	1.01	0.71	COBE + clusters

These cosmological models were chosen in order to put our ellipticity correlation measurements in context. The old standard cold dark matter model in which the universe is nearly closed by cold dark matter, is also disfavored in other observations. Its mass contrast is normalized to that found 300,000 years after the Big Bang via the cosmic microwave background radiation fluctuations (COBE). The other two models agree with a wide variety of observations, but only the cosmological constant (-dominated, at) cosmology also agrees with the recent evidence from supernova studies for accelerated expansion. b_b is the fraction of critical density in to ordinary (baryonic) matter. m_{matter} is the fraction in all matter (mostly dark matter), and σ_8 is the fraction in dark energy (the cosmological constant). H_0 is the Hubble constant in units of $\text{km s}^{-1} \text{Mpc}^{-1}$. The parameter n is the slope of the scale-free density power spectrum: $P(k) \propto k^n$, and σ_8 is the current mass contrast in a random sphere of radius $8(100=H_0) \text{ Mpc}$ compared with that for galaxies.³² The choice of $n=1$ and COBE normalization for standard cold dark matter results in too much mass fluctuation on galaxy cluster scales. By adjusting the slope n and current mass contrast σ_8 , models can be forced to fit the mass contrast now on galaxy cluster scales as well as the COBE normalization.

Figure 1: The distorted universe. Light rays from distant galaxies travel a tortuous path through a universe filled with clustering dark mass. Every bend in the path of a bundle of light from a distant galaxy stretches its apparent image. The orientation of the resulting elliptical images of galaxies contains information on the size and mass of the gravitational lenses distributed over the light path. The figure shows a schematic view of weak gravitational lensing by large-scale mass structure: distant galaxy orientation is correlated on scales characteristic of the lensing dark matter structures. Light bundles from two distant galaxies which are projected closely together on the sky follow similar paths and undergo similar gravitational deflections by intervening dark matter concentrations. Apparent orientations of distant galaxies are thus correlated on angular scales of less than a few degrees. The larger the mass in the gravitational defectors, the larger the faint galaxy ellipticity correlations on a given angular scale. These ellipticity correlations of distant galaxies reveal the statistics of the large-scale dark matter distribution in the intervening universe (a key diagnostic of the underlying cosmology).

Figure 2: Lens-induced galaxy orientation correlations. Pairs of background galaxies, separated on the sky by some angle, can have their relative orientations affected by weak lensing. The ellipticity components of any galaxy i with respect to galaxy j can be visualised as $e_1 = \cos(\theta)$ and $e_2 = \sin(\theta)$, where θ is the ellipticity and θ is the position angle with respect to a line joining the two galaxies. Ellipticity correlation functions are computed from the products of the ellipticity components of millions of such pairs, as a function of angular separation between pairs. A variety of relative orientations are illustrated along with their contributions to the correlations. Gravitational lensing leaves its signature on these correlations in several ways. First, the amplitude of the correlations scales with the amount of foreground mass. Second, the correlations are large at small separations and drop to nearly zero at large separations in a particular way. The bottom (red) case on the left cannot be caused by gravitational lensing, so that $e_1 e_1 i$ (averaged over many pairs) is always positive in the absence of systematic error. But lensing can cause the e_2 product to have either sign, as shown, and $e_2 e_2 i$ should become negative at a separation characteristic of the underlying cosmology. Third, correlations between e_1 and e_2 (not shown here) are not induced by gravitational lensing, so that any putative measurement of a lensing effect should vanish when galaxies are rotated by 45°.

Figure 3: Detection of ellipticity correlations. The panels show the mean of the ellipticity correlation functions ϵ_1 (left) and ϵ_2 (right) over the three fields (red), with 1 σ errors derived from the variance between fields. The behavior as a function of angle matches that expected from weak gravitational lensing by large-scale structure. The measurement errors in ϵ_1 and ϵ_2 are statistically independent. The faint galaxy ellipticity correlations are non-zero at 6 σ significance. The panels also contain two tests of systematic error. The cross-correlation $\langle \epsilon_1 \epsilon_2 \rangle$ averaged over the three fields is plotted as points (black squares) with 1 σ errors, while the ellipticity correlations of stars (blue stars) are also shown. Both are consistent with zero. In addition, a separate sample of faint red stars has ellipticity correlations consistent with zero. The galaxy ellipticity correlations continue to rise at smaller angles, but we cannot trust the 1 arcminute correlations due to apparent systematics in the few control stars on that angular scale. Additional tests of systematics, such as alignment with CCD axes, higher shear near edges, or patterns in the mass maps, are all null. The combined images and photometric catalogs are available (see supplementary information at www.nature.com).

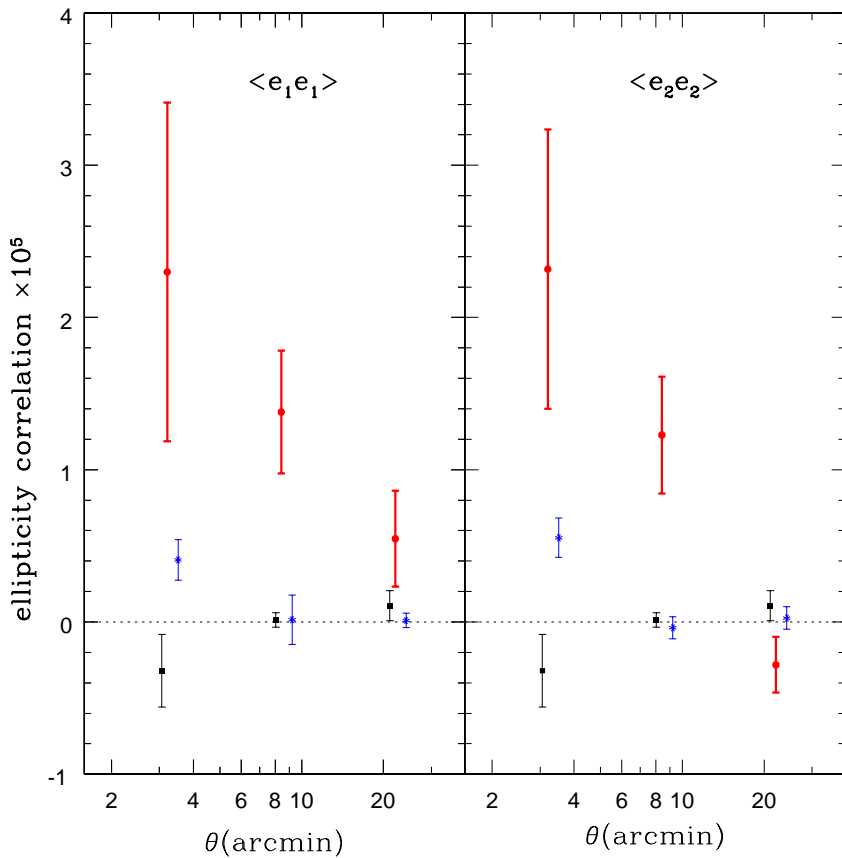
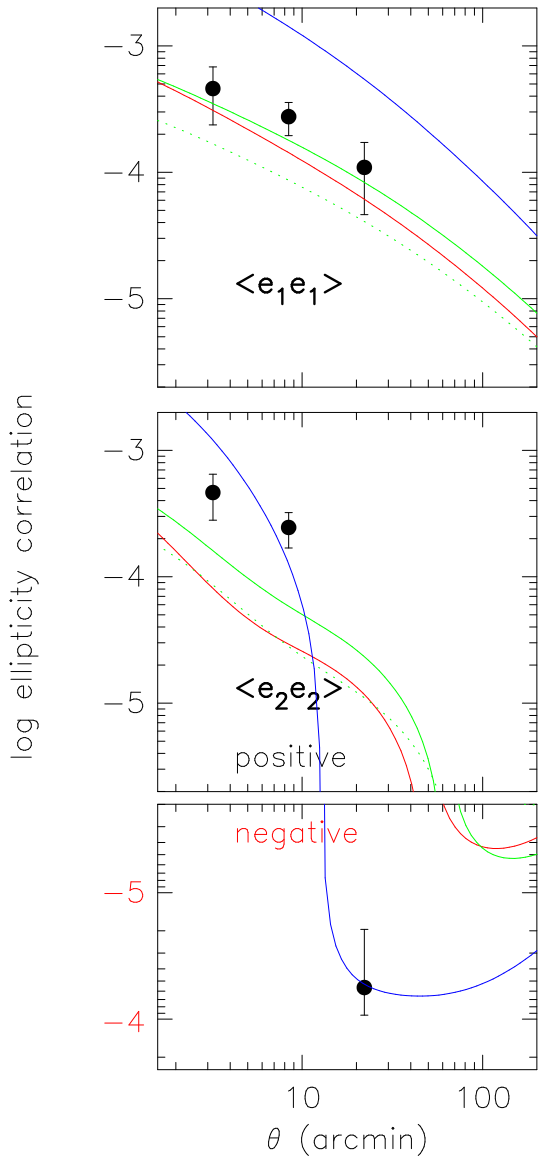


Figure 4: Comparison of ellipticity correlations with predictions. We plot our measurements with 1σ errors on a logarithmic scale along with theoretical predictions based on various models for a cold dark matter universe. The top theoretical curve is for the old standard cold dark matter model (blue) and the center and lower curves are for a universe with a cosmological constant (CDM, solid green) and an open universe (red), respectively. The dotted green curve shows the effect of decreasing the mode of the background galaxy redshift distribution, $2z_0$, from 1.0 to 0.6 for one model (CDM). The errors shown are derived from the variance among three fields, thus including statistical errors and cosmological variance, but not systematic errors. The data from Figure 3 have been multiplied by a correction factor of 20 here, to compensate for the factor of 4.5 dilution described in the text, which is squared in the correlation functions. Hence the systematic errors shown in Figure 3 are now at the few times 10^{-5} level. The 2σ measurements are consistent with all the models at the 2σ level, but standard cold dark matter is inconsistent with 1σ at many sigma. This first measurement of ellipticity correlations due to cosmological shear over half-degree angular scales is in agreement with a variety of other evidence in ruling out standard cold dark matter. Weak lens observations of larger fields and more distant galaxies will be able to clearly distinguish between the remaining models.



This figure "fig1.jpg" is available in "jpg" format from:

<http://arxiv.org/ps/astro-ph/0003014v1>

This figure "fig2.jpg" is available in "jpg" format from:

<http://arxiv.org/ps/astro-ph/0003014v1>